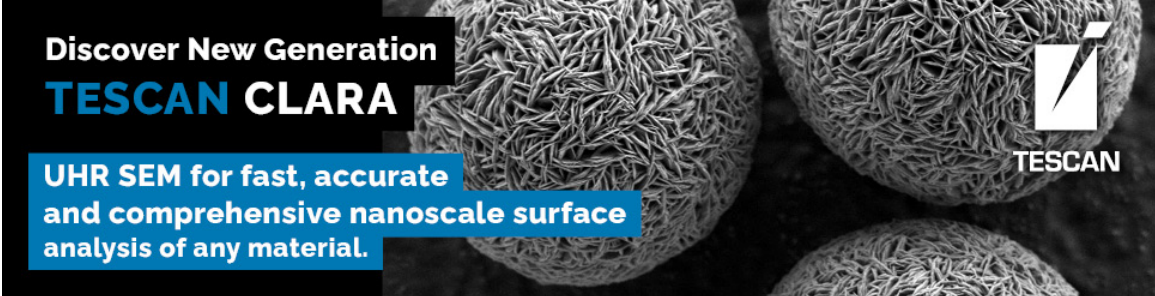



How Fast is Your Detector? The Effect of Temporal Response on Image Quality

Tiarnan Mullarkey, Matthew Geever, Jonathan J P Peters, Ian Griffiths, Peter D Nellist, Lewys Jones



Discover New Generation
TESCAN CLARA

UHR SEM for fast, accurate
and comprehensive nanoscale surface
analysis of any material.



TESCAN

How Fast is Your Detector? The Effect of Temporal Response on Image Quality

Tiarnan Mullarkey^{1,2,*} , Matthew Geever¹ , Jonathan J. P. Peters¹ , Ian Griffiths³,
Peter D. Nellist³ , and Lewys Jones^{1,4} 

¹School of Physics, Trinity College Dublin, College Green, Dublin D02 PN40, Ireland

²Centre for Doctoral Training in the Advanced Characterisation of Materials, AMBER Centre, Trinity College Dublin, Dublin D02 PN40, Ireland

³Department of Materials, University of Oxford, Parks Road, Oxford OX1 3PH, UK

⁴Advanced Microscopy Laboratory, Centre for Research on Adaptive Nanostructures and Nanodevices (CRANN), Trinity College Dublin, Dublin D02 PN40, Ireland

*Corresponding author: Tiarnan Mullarkey, E-mail: mullarkt@tcd.ie

Abstract

With increasing interest in high-speed imaging, there should be an increased interest in the response times of our scanning transmission electron microscope detectors. Previous works have highlighted and contrasted the performance of various detectors for quantitative compositional or structural studies, but here, we shift the focus to detector temporal response, and the effect this has on captured images. The rise and decay times of eight detectors' single-electron response are reported, as well as measurements of their flatness, roundness, smoothness, and ellipticity. We develop and apply a methodology for incorporating the temporal detector response into simulations, showing that a loss of resolution is apparent in both the images and their Fourier transforms. We conclude that the solid-state detector outperforms the photomultiplier tube-based detectors in all areas bar a slightly less elliptical central hole and is likely the best detector to use for the majority of applications. However, using the tools introduced here, we encourage users to effectively evaluate which detector is most suitable for their experimental needs.

Key words: high-speed imaging, low-dose imaging, scanning transmission electron microscopy (STEM), STEM detectors

Introduction

The scanning transmission electron microscope (STEM) has become a key piece of infrastructure in the toolkit of the modern researcher, ranging from biologists to material scientists (Pennycook & Nellist, 2011). This is perhaps largely due to its ability to produce readily interpretable images across a wide range of samples at varying magnifications using a finely focused electron beam (Fatermans et al., 2019; Dwyer, 2021). The necessity of using high energy electrons to achieve high resolution comes with the unavoidable consequence of associated damage to the samples being imaged. Avoiding damage is of great importance for imaging samples in their true state, or sometimes even at all, as losing a sample is regrettably common when imaging particularly fragile samples such as zeolites or biological specimens (Thach & Thach, 1971; Treacy & Newsam, 1987; Sartori Blanc et al., 1998; Egerton, 2019). An increasing understanding of these issues has also led to the enthusiastic development of sample damage mitigation strategies such as cryogenic holders, and particularly, a move away from long, slow scan-frames toward higher-speed, multiframe data sets (Jones et al., 2015; Ophus et al., 2016; Jones et al., 2018; Mullarkey et al., 2022).

This ever-growing interest in low-dose (here measured in $e^-/\text{Å}^2$) STEM imaging has led to fast-scanning multiframe acquisition strategies becoming increasingly commonplace. While lowering the beam current decreases the electron

dose, it is by fast scanning that we can also decrease the electron *dose rate*, which can be the more relevant factor than just total dose for many materials (Jiang & Spence, 2012; Johnston-Peck et al., 2016; Jones et al., 2018; Egerton, 2019). Although shorter dwell times inherently lead to lower signal-to-noise ratios (SNRs) due to less signal collection, what may be less obvious is that previously largely unreported artifacts also begin to appear. The most apparent of these is signal streaking, which becomes visible when the decay time of the scintillator from single-electron impact events is greater than or of a similar duration to the dwell time being used (Buban et al., 2010; Jones & Downing, 2018; Mullarkey et al., 2020). Hence, as low-dose and dose-rate imaging becomes more important, so too does the high-speed performance characteristics of the detector that is used.

Previously with an emphasis on structural studies, we have stressed the importance of the flatness of the detector used (Macarthur et al., 2014). Now, with an interest in speed, we seek to revisit and update that earlier work for the community in the context of temporal response, while also including a new solid-state detector. Therefore, the aims of this paper are to explore the origin and effects of this signal streaking and to compare the performance of a range of detectors available today. By doing so, we hope to inform instrument users, purchasers, and detector manufacturers of the significance of these effects and the best conditions under

Received: December 8, 2022. Revised: March 8, 2023. Accepted: May 13, 2023

© The Author(s) 2023. Published by Oxford University Press on behalf of the Microscopy Society of America.

This is an Open Access article distributed under the terms of the Creative Commons Attribution License (<https://creativecommons.org/licenses/by/4.0/>), which permits unrestricted reuse, distribution, and reproduction in any medium, provided the original work is properly cited.

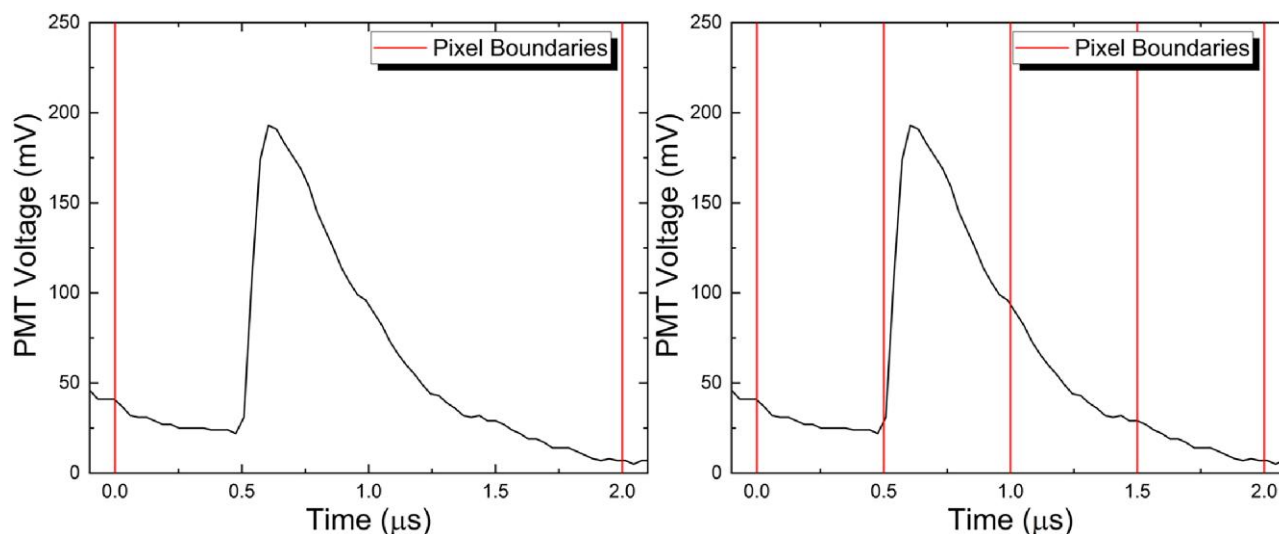


Fig. 1. Signal streaking may occur at any dwell time, although it is rarely seen at dwell times that are longer than the decay time of the pulse, such as on the left. However, it becomes increasingly common at shorter dwell times, and eventually inescapable, such as on the right.

which an instrument is to be operated so as to minimize these effects.

Background

Image Formation in the STEM

To understand signal streaking, we first discuss image formation in the STEM. While TEM imaging uses broad-beam illumination of the sample to form an image directly on a CCD camera or photographic plate, STEM imaging uses a finely focused electron probe scanned in a raster fashion. The electron probe spends a fixed amount of time at each pixel (the pixel dwell time) collecting signals of interest using various detectors [e.g., annular dark-field (ADF), bright-field (BF), and energy dispersive X-ray spectroscopy detectors]. In the specific case of ADF detectors, the focus of this work, electrons are collected, which have been scattered to a range of angles by the sample being studied. Electrons that are scattered to high angles have undergone Rutherford scattering by the sample's nuclei. Therefore, heavier nuclei or thicker sample regions result in more scattering, and in turn, brighter pixels. Images produced this way are commonly referred to as having Z-contrast or mass-thickness contrast. This is an incoherent, easily interpretable imaging mode, which has led to its wide use by many (Nellist & Pennycook, 2000; Jones, 2016).

At every pixel, the output of the detector is captured, returning the average value of the detector's output during the dwell time, and producing the arbitrary pixel values we see in the image. Recently, pixelated STEM detectors have also been developed, but these operate orders of magnitude slower than scintillator-photomultiplier types (dwell times of tens or hundreds of microseconds, as opposed to tens of nanoseconds) and hence are not the focus of this work. An important aspect of the beam rastering in STEM is that the image formed is *not* from a simultaneous acquisition mode, so each pixel has been captured at a different point in time. Hence, STEM images are particularly susceptible to some well-known time-varying sources of noise, such as sample drift (whether mechanical or thermal) and stray electromagnetic fields, and other

environmental sources such as acoustic disturbances (von Harrach, 1995; Jones & Nellist, 2013).

A lesser known time-dependent artifact arises due to the decay time of nonideal detectors and the corresponding readout electronics. A common setup is to use a scintillator-photomultiplier tube (PMT)-based detector with a scintillating crystal such as yttrium aluminum perovskite (YAP). In such a system, an electron that impinges on the scintillating crystal generates numerous photons that travel along a light guide. These photons are then converted back to electrons via the photoelectric effect and are accelerated toward successive dynodes. At each dynode, an accelerated electron has enough energy to liberate numerous other electrons upon collision, and in this way, a single initial electron hitting the detector can produce millions of electrons, and therefore a readily detectable output signal (Ishikawa et al., 2014; Sang & LeBeau, 2016).

While YAP may have a decay time as low as 25 ns (Baccaro et al., 1995; Novák & Müllerová, 2009), when in combination with the photomultiplier and readout electronics, it is not uncommon to see decay times $>1 \mu\text{s}$ associated with the event from a single-electron impact (Sang & LeBeau, 2016; Mittelberger et al., 2018; Mullarkey et al., 2020). If this decay time is greater than, or of a similar duration to, the pixel dwell time, we begin to see the “streaking” of the signal between neighboring pixels (Fig. 1), which has also been observed in other literature (Buban et al., 2010). While dwell times $< \sim 1 \mu\text{s}$ are not often used, newer scan generators can achieve dwell times of 50 ns, e.g., point Electronic's DISS 6 and the Gatan DigiScan 3, and so signal streaking will become both more relevant, and severe, as these become more widespread.

This streaking results in a loss of high-resolution information in the image, which is also observable in the Fourier transform as a drop in intensity of the higher spatial frequency Fourier components. This effect reduces the accuracy and precision of STEM images in which it is present, as signal that should be localized entirely to one pixel is instead assigned to neighboring pixels. Furthermore, as this is a temporal effect, it is independent of magnification and persists across images captured at varying length scales.

A further issue is that the response of the detector to electrons of the same energy is not homogenous. This is well known, and many detectors have had their responses quantified using metrics such as flatness, roundness, smoothness, and ellipticity (Macarthur et al., 2014). Some of these intensity variations in the response are inherent due to the asymmetric position of the readout electronics with respect to the detector or the presence of a hole through the center of the scintillator. Others are due to issues that could be fixed at the manufacturing level, such as by combining the usual scintillating crystal with a layer of P47 scintillator to increase detection efficiency (Kaneko et al., 2014). Since the early days of STEM people discovered, it was possible to do quantitative structural studies even with detectors that have large intensity variations (Singhal et al., 1997). Despite these known inhomogeneities, these detector imperfections persist through to other studies, with these detectors still being installed on machines to this day. To compensate for these effects, an operator will often directly capture an image of the detector (referred to as a detector scan or map) just before or after an experiment at the same conditions used for capturing the data. The detector response at these conditions is then used to normalize the data after subtraction of the dark level, allowing for easier comparison with simulations (Grieb et al., 2012; Mehrtens et al., 2013). A recent review of the literature in this field is presented in Jones (2020).

While there have been approaches to remedy signal streaking such as signal shifting or the digitization of the raw signal from the detector, we understand that these approaches are not available to all (Jones & Downing, 2018; Mullarkey et al., 2020). Instead of focusing on the methods of removing streaking from images, we shift the focus to quantifying the effects this streaking has on images and the performance of different detectors on the market.

Materials and Methods

Capturing Single-Electron Signals

Understanding the decay behavior of a detector requires observing the detector's response to single electrons. The method to achieve a low enough dose at the detector to see this signal may vary depending on the configuration of the microscope, i.e., one can lower the extraction on a STEM with a cold field-emission gun (FEG) easily, while a STEM equipped with a Schottky FEG cannot simply lower the extraction. Instruments with monochromators are also easily able to reduce beam current by reducing the energy range of electrons that can pass. In the case of ADF detectors, moving the electron beam to a thin or low-mass region of the sample to reduce the amount of scattering to the detector and reducing the camera length such that most scattered electrons instead pass through the central hole are other widely available options. Although these are not ideal efficient operating conditions for imaging, they are suitable for collecting a weak signal for testing.

As image formation involves processing the detector output signal at each pixel, the raw trace of a single-electron pulse is not preserved in the final image. Accessing this instead requires the use of an oscilloscope or similar. In this work, pulses shown have either been captured on a PicoScope 2000 USB-streaming oscilloscope or a Red Pitaya measurement board. Where the raw data are accessed also depends on the microscope configuration. In some cases, the detector can be connected to directly (using, e.g., a BNC connector), and if a microscope is controlled by an external scan controller (i.e.,

point electronic DISS6 or Gatan DigiScan), it is possible to intercept the signal close to the scan controller inputs. To accurately capture an electron pulse, it is sometimes necessary to adjust the brightness and gain to ensure no clipping, high or low, of the signal, as well as a suitably large signal to background ratio. Having captured a single pulse, it can then be analyzed with respect to its rise times and decay times.

Detector Scans

Observing a pulse directly contains information on *how* the intensity response of a detector to a single electron varies, and only by capturing detector scan, can it be revealed *why*. The method for obtaining detector scans again varies with instrument, although necessarily starts with moving to a region of vacuum in the sample so the detector can be imaged directly. The beam must then be focused at the detector plane, which can be achieved by switching to diffractive or confocal mode while the detector is inserted. It is recommended to discuss with a technician for the instrument of interest if you wish to perform a detector scan, as incorrect setup may temporarily "burn" the detector surface. These detector scans are analyzed by calculating the flatness, roundness, smoothness, and ellipticity of each, as defined in Macarthur et al. (2014). These definitions are reproduced here for ease of reading, and our code implementation to evaluate these parameters is linked in the section Availability of Data and Materials.

- Flatness: Detector sensitivity with respect to scattering angle (radially) after averaging azimuthally.
- Roundness: A measure of the consistency of the detector sensitivity around the detector (azimuthally) after averaging radially.
- Smoothness: The full-width-quarter-maximum of the active region of the normalized histogram.
- Ellipticity: The percentage of the major over the minor diameters of the inner-angle opening.

Simulation

To not only investigate the sources of image streaking but also to simulate its effects, code was developed to reproduce electron pulses and artificially streak simulated images. This process starts by producing a simulation with known fractional scattering of the beam at each pixel, using software such as Prismatic 2.0 (Rangel DaCosta et al., 2021). For a known electron dose, this fractional scattering can be converted to a number of electron impacts per pixel. These impacts follow a Poisson distribution in time (Sang & LeBeau, 2016) and can have (for example) Gaussian distributed intensities to emulate detector inhomogeneity. The simulated pulse shape is then assigned at each generated time stamp following these distributions. The average pixel intensity value is calculated, and an image with the effects of signal streaking is produced. By changing the starting simulation, simulated pulse shape, dwell time, and pulse intensity distribution, images that account for detector performance can now be simulated and studied relative to a known ground truth.

Results and Discussion

Detector Scans

Detector scans from eight detectors produced by five different manufacturers were captured: one BF detector, six PMT-based

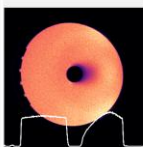
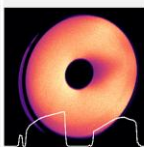

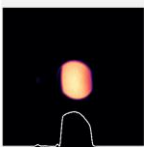
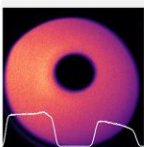
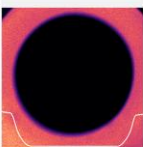
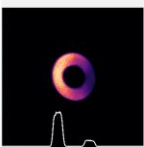
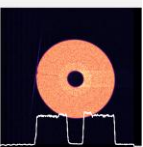
	Company 1	Company 2			Company 3		Company 4	Company 5
	Detector A (ADF)	Detector B (ADF)	Detector C (ADF)	Detector D (BF)	Detector E (ADF)	Detector F (ADF)	Detector G (ADF)	Detector I (SEG)
Detector Map & Profile								
Flatness	9.86%	6.69%	9.61%	8.97%	8.38%	4.07%	21.60%	2.94%
Roundness	5.08%	5.42%	6.63%	6.27%	15.95%	5.77%	49.64%	1.34%
Smoothness	29.77%	51.76%	42.55%	51.19%	58.50%	33.16%	149.81%	22.62%
Ellipticity	1.88%	12.37%	2.81%	-	4.90%	1.88%	10.69%	2.82%

Fig. 2. Detector maps of the detectors used to capture individual pulses in figure 3 overlaid with their intensity profiles. Flatness, roundness, smoothness, and ellipticity measurements are tabulated below, with these values given as a measure of the deviation from a perfect detector, where 0% would be a perfect match. The detector type is noted in brackets, where SEG is short for segmented detector. We choose not to show company names, but we encourage users to perform analysis themselves on their own system.

ADF detectors, and one solid-state segmented annular detector (Fig. 2). A large variety in their responses can be seen qualitatively, and this is also evidenced in the intensity profiles that are captured from across the center of each detector. In some, we see an asymmetric response, which may imply that this is being caused by the placement of the readout electronics. For example, we know the light guide and PMT for detector A are located on the left-hand side as presented in the image. Correspondingly, we see a region of low sensitivity on the right-hand side of the central hole, as many photons produced here are unable to navigate around the hole and reach the PMT. Similar behavior can be seen across many of the other detectors.

When comparing these detectors using the previously defined metrics, we see that no single detector performs best across every category. To first compare scintillator-photomultiplier tube-based detectors against each other we see that while detector A is the most round and smooth and tied for least elliptical, it is one of the least flat detectors. If compositional studies are important than this detector may be ill-advised due its poor flatness, despite its otherwise strong performance. For quantitative studies where comparisons with simulation will be used having a well-defined inner-angle is extremely important, and so detectors with large ellipticity values cannot be recommended. Note that ellipticity is undefined for the BF detector as it is defined relative to the inner angles in this study.

The solid-state detector outperforms the rest in every category except ellipticity. As electrons are converted directly to charge in this style of detector many of the problems and challenges associated with photomultiplier-based readouts are absent. However, there are defined channels through which the detector outputs are read, which result in very thin dead zones, perhaps impacting some detection efficiency. It can also be seen that the inner four rings of the segmented detector appear brighter than the outer rings; however, such an offset could be eliminated with a gain reference at the beginning of an experiment.

Electron Pulses

We show here a comparison of individual pulses captured from some of the detectors presented above and discuss their 10–90% rise and decay times and other characteristics (Fig. 3). We choose the rise and decay times to discuss as

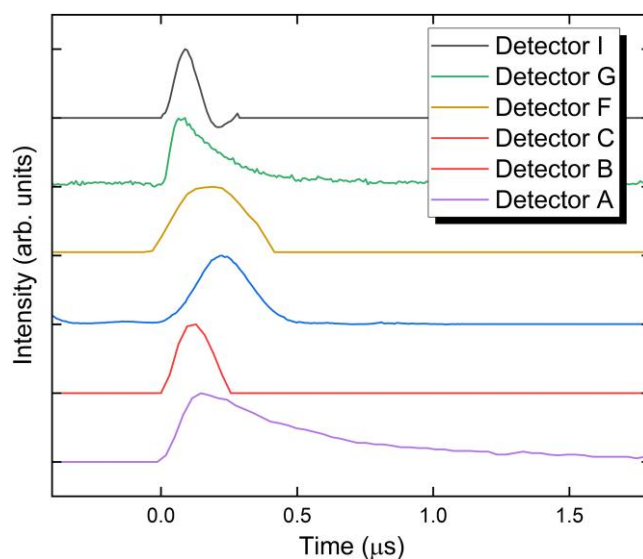


Fig. 3. Example of single electron impacts from six different STEM ADF detectors spanning five different manufacturers, with the model specified by the letter in brackets. The intensity of a pulse varies due to detector inhomogeneity and gain, but each has been normalized here for comparative purposes. Some pulses have artificially flat backgrounds due to how the pulse profile was extracted from its respective data stream.

they can be intuitively related to important aspects of image degradation.

There are broadly two pulse shapes seen: a sharp rising edge followed by an exponential decay, and a more symmetric, Lorentzian/Gaussian pulse shape. While the former is perhaps more naturally understood as being caused by the electron–detector interaction, the latter may be due to shaping amplifiers, often used where preserving the area under the curve is important in applications such as spectrometers (Buzzetti et al., 2003).

In the case of the symmetric pulse-shape both rise time and decay time are important parameters when evaluating the likelihood, and severity, of pixel streaking. For the exponential decay shape, the decay time is often an order of magnitude larger than the rise time and is more significant when it comes to the severity of the streaking (Fig. 4). The rise time, however, has

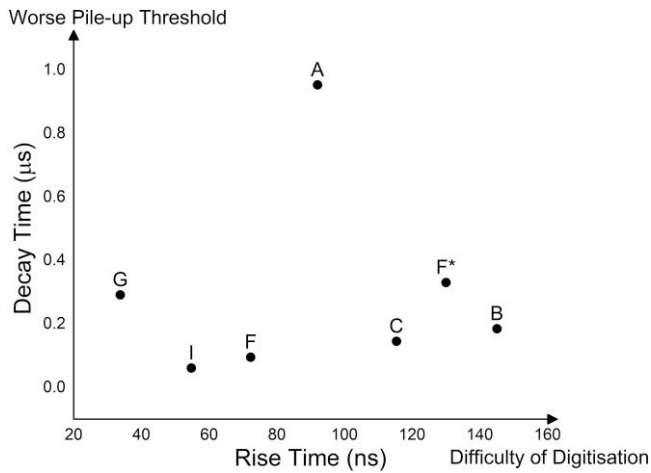


Fig. 4. Typical values for the 10–90% rise times (in ns) and decay times (in μs) of pulses were calculated and are plotted here for the same detectors used to capture pulses in figure 3. The closer a point is to the origin the less likely it is to streak, and the less severe the streaking will be if it occurs.

another piece of significance. Should one look to digitization approaches having a sharp feature such as a very short rise time can aid in electron detection, and this can counteract the drawbacks caused by the decay time (Mullarkey et al., 2020).

It was also noted that the shape of a pulse can depend on where it is captured from the instrument. This may be due to effects such as impedance matching and is seen here with two pulse sizes reported for detector F, with an example shown in Mullarkey et al. (2020). Although it may not be possible to take advantage of this fact, it is important to note for precise reporting of electron pulse sizes in the literature.

Simulation

Having captured example electron pulses the first goal was to create a model of these. As an example, a lognormal distribution was used to recreate the pulse shape of detector A, shown in Figure 5 alongside the experimental signal.

This simulated pulse shape was then incorporated into a simulation using a beam current of 5 pA. The results of this are shown in Figure 6 for simulations with dwell times of 1 μs , 200, 100, and 50 ns, with this chosen as the shortest dwell time as it corresponds to the speed attainable on new generation scan generators. As the simulated pulse has a decay time $>1 \mu\text{s}$, it is expected that streaking will be present in all images, but significantly more severe in the images with lower dwell times. This behavior is indeed seen in the images, with streaking occurring across multiple pixels being obvious in the 200, 100, and 50 ns dwell-time images. Although visually obvious, the Fourier transform can also be used as further evidence of image degradation. The Fourier transforms are presented in the lower row of the image, with one notable feature appearing as we move to shorter dwell times: a drop in intensity of the higher spatial frequency Fourier components in the fast-scanning direction. This can be understood as the streaking resulting in a loss of high-frequency information in the images, reflected in this frequency envelope in the Fourier transform. It is worth reiterating that as this is a temporal effect, and not spatial, it does not only effect higher

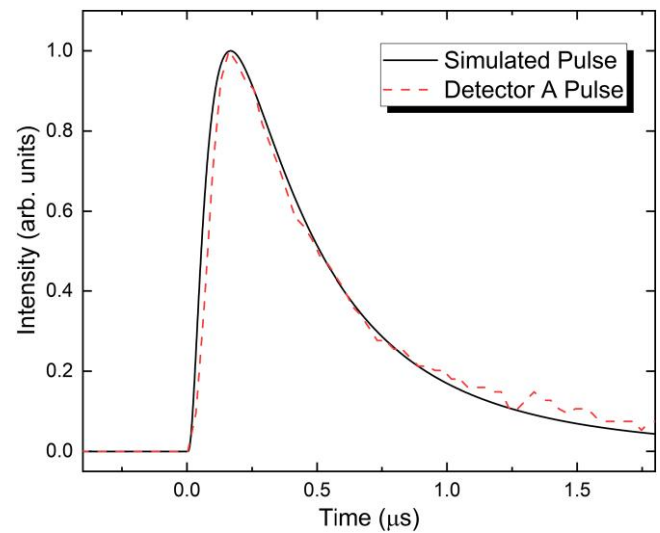


Fig. 5. An example of an electron pulse captured from detector A (dashed), and our simulated model of it (solid).

magnification images. Sharp image features (a few pixels in size in the fast-scan direction) regardless of physical size, can be obfuscated by this streaking, and valuable information lost. We leave this study purely simulation based to isolate the effects of signal streaking from other sources of experimental noise/distortions. This is of particular importance as images captured at low doses and high speeds have low SNRs, and these other sources of noise make it difficult to separate *only* the effects of detector response.

Conclusions

In this paper, we have shown single-electron signals captured from various detectors and corresponding detector maps to highlight some of the issues caused directly by detector hardware, namely signal streaking and detector inhomogeneity. It is seen that pulses can vary between having sudden onsets and exponential decays, or symmetrical pulse shapes, perhaps due to the use of shaping amplifiers. The duration of these pulses varies both when comparing between technologies (PMT versus solid state), or even within the same class of detector. Rise times ranged from ~ 30 to 150 ns, and decay times from ~ 0.1 to 0.9 μs for the pulses shown in this paper.

When comparing detector maps, it was seen that no single detector outperformed in all metrics measured, although some do lead in certain categories. While detector A performs best in smoothness, roundness, and ellipticity and may appear a good choice, it also has a decay time more than twice as long as the other detectors, and therefore, the worst high-speed performance. The solid-state detector outperforms in all categories but in the ellipticity of its central hole (and even then, is only marginally worse), indicating that this is the nearest detector to an ideal case and that solid-state detection leads to a marked improvement in performance. It is important to balance the contributions of the factors described in this paper when choosing a suitable detector for specific experimental uses.

Finally, by bringing these factors into simulations, we have produced images containing streaking as it would appear on a detector A for a range of dwell times. At shorter dwell times, we see obvious streaking between neighboring pixels, and

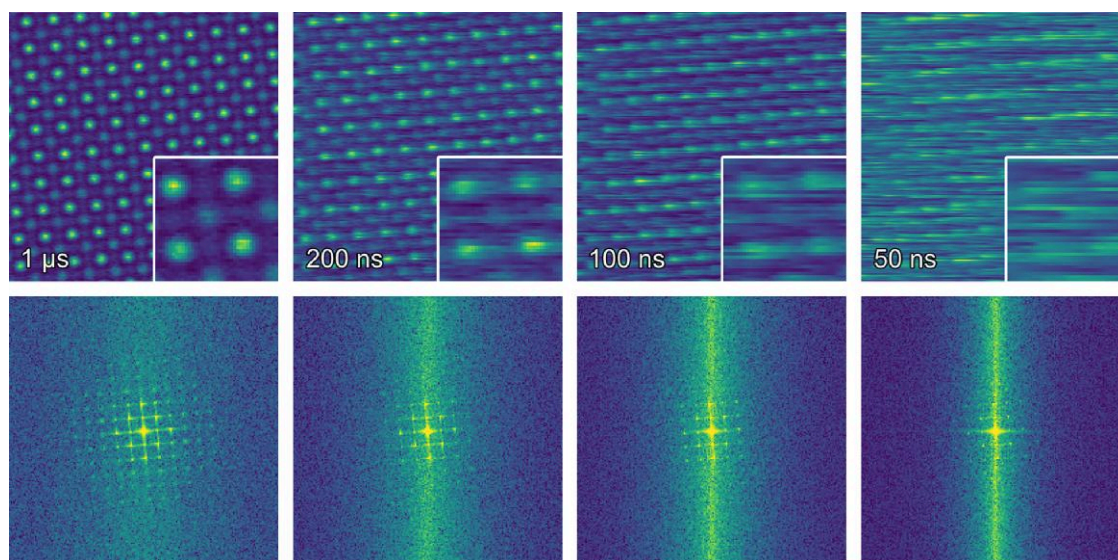


Fig. 6. Four simulated streaked images of strontium titanate (SrTiO_3) using a beam current of 5 pA are shown in the top row with dwell times 1 μs , 200 ns, 100 ns, and 50 ns, respectively. The pulse shape used to simulate the streaking is that shown in Figure 5. Below each image is its corresponding Fourier transform.

correspondingly, a drop in the intensity at higher spatial frequencies in the Fourier transform. Even if streaking may not be visually obvious such as in the 1 μs dwell-time simulation, this drop in intensity is still present in the Fourier transform. By providing tools to properly characterize detector speeds, we hope to enable performance evaluation of detectors at the manufacturing level, or by prospective purchasers to gauge if the detector's performance will be suitable for their imaging needs. We also envision that as new scan generators that can scan an order of magnitude faster become more widely available, such evaluations will become increasingly more important should one want to produce images of acceptable quality at these now accessible speeds.

Availability of Data and Materials

The Python code used to produce the flatness, roundness, smoothness, and ellipticity measurements for the detectors in Figure 2 is available in the following link <https://github.com/TCD-Ultramicroscopy/How-flat-is-your-detector>.

Acknowledgments

The authors acknowledge the Centre for Research on Adaptive Nanostructures and Nanodevices (CRANN) and the Advanced Materials and BioEngineering Research (AMBER) Network for financial and infrastructural support for this work. J.J.P.P. and L.J. acknowledge SFI grant 19/FFP/6813, T.M. acknowledges the SFI & EPSRC Centre for Doctoral Training in the Advanced Characterisation of Materials (award references 18/EPSRC-CDT-3581 and EP/S023259/1). This project has received funding from the European Union's Horizon 2020 research and innovation program under grant agreement number 823717-ESTEEM3.

Financial Support

The current study hasn't received any fund from any organizations or institutions.

Conflict of Interest

The authors declare that they have no competing interests.

References

- Baccaro S, Blažek K, de Notaristefani F, Maly P, Mares J, Pani R, Pellegrini R & Soluri A (1995). Scintillation properties of YAP:Ce. *Nucl Instr Methods Phys Res Sect A: Accel Spectrom Detect Assoc Equip* 361, 209–215. [https://doi.org/10.1016/0168-9002\(95\)00016-X](https://doi.org/10.1016/0168-9002(95)00016-X)
- Buban JP, Ramasse Q, Gipson B, Browning ND & Stahlberg H (2010). High-resolution low-dose scanning transmission electron microscopy. *J Electron Microscop (Tokyo)* 59, 103–112. <https://doi.org/10.1093/jmicro/dfp052>
- Buzzetti S, Guazzoni C & Longoni A (2003). EROIC: A BiCMOS pseudo-Gaussian shaping amplifier for high-resolution X-ray spectroscopy. *Nucl Instrum Methods Phys Res Sect A: Accel Spectrom Detect Assoc Equip* 512, 150–156. [https://doi.org/10.1016/S0168-9002\(03\)01889-8](https://doi.org/10.1016/S0168-9002(03)01889-8)
- Dwyer C (2021). Quantitative annular dark-field imaging in the scanning transmission electron microscope—A review. *J Phys: Mater* 4, 042006. <https://doi.org/10.1088/2515-7639/ac1ab8>
- Egerton RF (2019). Radiation damage to organic and inorganic specimens in the TEM. *Micron* 119, 72–87. <https://doi.org/10.1016/j.micron.2019.01.005>
- Fatemi J, Van Aert S & den Dekker AJ (2019). The maximum a posteriori probability rule for atom column detection from HAADF STEM images. *Ultramicroscopy* 201, 81–91. <https://doi.org/10.1016/j.ultramic.2019.02.003>
- Grieb T, Müller K, Fritz R, Schowalter M, Neugebohrn N, Knaub N, Volz K & Rosenauer A (2012). Determination of the chemical composition of GaNAs using STEM HAADF imaging and STEM strain state analysis. *Ultramicroscopy* 117, 15–23. <https://doi.org/10.1016/j.ultramic.2012.03.014>
- Ishikawa R, Lupini AR, Findlay SD & Pennycook SJ (2014). Quantitative annular dark field electron microscopy using single electron signals. *Microsc Microanal* 20, 99–110. <https://doi.org/10.1017/S1431927613013664>
- Jiang N & Spence JCH (2012). On the dose-rate threshold of beam damage in TEM. *Ultramicroscopy* 113, 77–82. <https://doi.org/10.1016/j.ultramic.2011.11.016>

- Johnston-Peck AC, DuChene JS, Roberts AD, Wei WD & Herzing AA (2016). Dose-rate-dependent damage of cerium dioxide in the scanning transmission electron microscope. *Ultramicroscopy* 170, 1–9. <https://doi.org/10.1016/j.ultramic.2016.07.002>
- Jones L (2016). Quantitative ADF STEM: Acquisition, analysis and interpretation. *IOP Conf Ser: Mater Sci Eng* 109, 012008. <https://doi.org/10.1088/1757-899X/109/1/012008>
- Jones L (2020). Practical aspects of quantitative and high-fidelity STEM data recording. In *Scanning Transmission Electron Microscopy*, Bruma A (Ed.), pp. 1–40. Boca Raton, FL: CRC Press.
- Jones L & Downing C (2018). The MTF & DQE of annular dark field STEM: Implications for low-dose imaging and compressed sensing. *Microsc Microanal* 24, 478–479. <https://doi.org/10.1017/S143192761800288X>
- Jones L & Nellist PD (2013). Identifying and correcting scan noise and drift in the scanning transmission electron microscope. *Microsc Microanal* 19, 1050–1060. <https://doi.org/10.1017/S1431927613001402>
- Jones L, Varambhia A, Beanland R, Kepaptsoglou D, Griffiths I, Ishizuka A, Azough F, Freer R, Ishizuka K, Cherns D, Ramasse QM, Lozano-Perez S & Nellist PD (2018). Managing dose-, damage- and data-rates in multi-frame spectrum-imaging. *Microscopy* 67, 98–113. <https://doi.org/10.1093/jmicro/dfx125>
- Jones L, Yang H, Pennycook TJ, Marshall MSJ, Van Aert S, Browning ND, Castell MR & Nellist PD (2015). Smart align—A new tool for robust non-rigid registration of scanning microscope data. *Adv Struct Chem Imaging* 1, 1–16. <https://doi.org/10.1186/s40679-015-0008-4>
- Kaneko T, Saitow A, Fujino T, Okunishi E & Sawada H (2014). Development of a high-efficiency DF-STEM detector. *J Phys: Conf Ser* 522, 012050. <https://doi.org/10.1088/1742-6596/522/1/012050>
- Macarthur KE, Jones LB & Nellist PD (2014). How flat is your detector? Non-uniform annular detector sensitivity in STEM quantification. *J Phys: Conf Ser* 522, 1198–1199. <https://doi.org/10.1088/1742-6596/522/1/012018>
- Mehrtens T, Schowalter M, Tytko D, Choi P, Raabe D, Hoffmann L, Jönen H, Rossow U, Hangleiter A & Rosenauer A (2013). Measurement of the indium concentration in high indium content InGaN layers by scanning transmission electron microscopy and atom probe tomography. *Appl Phys Lett* 102, 132112. <https://doi.org/10.1063/1.4799382>
- Mittelberger A, Kramberger C & Meyer JC (2018). Software electron counting for low-dose scanning transmission electron microscopy. *Ultramicroscopy* 188, 1–7. <https://doi.org/10.1016/j.ultramic.2018.02.005>
- Mullarkey T, Downing C & Jones L (2020). Development of a practicable digital pulse read-out for dark-field STEM. *Microsc Microanal* 27, 99–108. <https://doi.org/10.1017/S1431927620024721>
- Mullarkey T, Peters JJP, Downing C & Jones L (2022). Using your beam efficiently: Reducing electron dose in the STEM via flyback compensation. *Microsc Microanal* 28, 1428–1436. <https://doi.org/10.1017/S1431927621013908>
- Nellist PD & Pennycook SJ (2000). The principles and interpretation of annular dark-field Z-contrast imaging. *Adv Imaging Electron Phys* 113, 147–203. [https://doi.org/10.1016/S1076-5670\(00\)80013-0](https://doi.org/10.1016/S1076-5670(00)80013-0)
- Novák L & Müllerová I (2009). Single electron response of the scintillator-light guide-photomultiplier detector. *J Microsc* 233, 76–83. <https://doi.org/10.1111/j.1365-2818.2008.03096.x>
- Ophus C, Ciston J & Nelson CT (2016). Correcting nonlinear drift distortion of scanning probe and scanning transmission electron microscopies from image pairs with orthogonal scan directions. *Ultramicroscopy* 162, 1–9. <https://doi.org/10.1016/j.ultramic.2015.12.002>
- Pennycook SJ & Nellist PD (2011). *Scanning Transmission Electron Microscopy*, Pennycook, SJ & Nellist, PD (Eds.), pp. 1–90. New York, NY: Springer.
- Rangel DaCosta L, Brown HG, Pelz PM, Rakowski A, Barber N, O'Donovan P, McBean P, Jones L, Ciston J, Scott MC & Ophus C (2021). Prismatic 2.0—Simulation software for scanning and high resolution transmission electron microscopy (STEM and HRTEM). *Micron* 151, 103141. <https://doi.org/10.1016/j.micron.2021.103141>
- Sang X & LeBeau JM (2016). Characterizing the response of a scintillator-based detector to single electrons. *Ultramicroscopy* 161, 3–9. <https://doi.org/10.1016/j.ultramic.2015.11.008>
- Sartori Blanc N, Studer D, Ruhl K & Dubochet J (1998). Electron beam-induced changes in vitreous sections of biological samples. *J Microsc* 192, 194–201. <https://doi.org/10.1046/j.1365-2818.1998.00420.x>
- Singhal A, Yang JC & Gibson JM (1997). STEM-based mass spectroscopy of supported Re clusters. *Ultramicroscopy* 67, 191–206. [https://doi.org/10.1016/S0304-3991\(96\)00094-0](https://doi.org/10.1016/S0304-3991(96)00094-0)
- Thach RE & Thach SS (1971). Damage to biological samples caused by the electron beam during electron microscopy. *Biophys J* 11, 204–210. [https://doi.org/10.1016/S0006-3495\(71\)86208-2](https://doi.org/10.1016/S0006-3495(71)86208-2)
- Treacy MMJ & Newsam JM (1987). Electron beam sensitivity of zeolite L. *Ultramicroscopy* 23, 411–419. [https://doi.org/10.1016/0304-3991\(87\)90252-X](https://doi.org/10.1016/0304-3991(87)90252-X)
- von Harrach HS (1995). Instrumental factors in high-resolution FEG STEM. *Ultramicroscopy* 58, 1–5. [https://doi.org/10.1016/0304-3991\(94\)00172-J](https://doi.org/10.1016/0304-3991(94)00172-J)



TESCAN TENSOR

Integrated, Precession-Assisted,
Analytical 4D-STEM



Visit us and learn more
about our TESCAN TENSOR

info.tescan.com/stem